

# Capturing snapshots of post-synthetic metallation chemistry in metal-organic frameworks

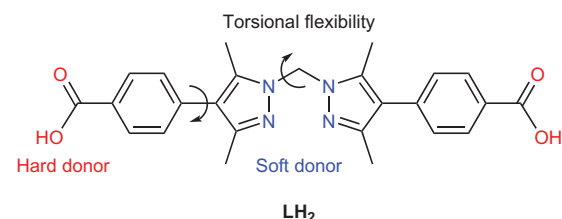
Witold M. Bloch<sup>1</sup>, Alexandre Burgun<sup>1</sup>, Campbell J. Coghlan<sup>1</sup>, Richmond Lee<sup>2</sup>, Michelle L. Coote<sup>2</sup>, Christian J. Doonan<sup>1\*</sup> and Christopher J. Sumby<sup>1\*</sup>

**Post-synthetic metallation is employed strategically to imbue metal-organic frameworks (MOFs) with enhanced performance characteristics. However, obtaining precise structural information for metal-centred reactions that take place within the pores of these materials has remained an elusive goal, because of issues with high symmetry in certain MOFs, lower initial crystallinity for some chemically robust MOFs, and the reduction in crystallinity that can result from carrying out post-synthetic reactions on parent crystals. Here, we report a new three-dimensional MOF possessing pore cavities that are lined with vacant di-pyrazole groups poised for post-synthetic metallation. These metallations occur quantitatively without appreciable loss of crystallinity, thereby enabling examination of the products by single-crystal X-ray diffraction. To illustrate the potential of this platform to garner fundamental insight into metal-catalysed reactions in porous solids we use single-crystal X-ray diffraction studies to structurally elucidate the reaction products of consecutive oxidative addition and methyl migration steps that occur within the pores of the Rh-metallated MOF, 1-[Rh(CO)<sub>2</sub>][Rh(CO)<sub>2</sub>Cl<sub>2</sub>].**

Singl-crystal X-ray diffraction (SCXRD) is a powerful and ubiquitous technique used to definitively elucidate molecular structure<sup>1,2</sup>. One of the fundamental requirements for obtaining a structure solution from a diffraction pattern is the presence of long-range order of electron density within the crystal. A consequence of this experimental constraint is that the precise observation of guests within the cavities of porous solid-state materials is a significant challenge due to partial site occupancy and disorder. Recent work by the Fujita group demonstrated that metal-organic frameworks (MOFs) are suitable host matrices for isolating and unambiguously characterizing the structure and relative stereochemistry of ordered guest molecules on a nanogram scale<sup>3</sup>. This elegant work builds upon earlier efforts that utilize solid-state materials with defined cavities to stabilize and crystallographically characterize reactive organic compounds<sup>4–8</sup> and organometallic moieties<sup>9,10</sup>. In addition, the adsorption of gas molecules within MOFs has been analysed by SCXRD methods to yield detailed information on binding modes and preferred adsorption sites<sup>11–14</sup>. This body of preceding work clearly demonstrates that MOFs are a versatile platform for characterizing molecular guest species in the solid-state.

Recently, Fujita's 'crystalline sponges' have been used to elucidate the structure of a trifluoromethylthiolation reagent<sup>15</sup> and to study the reactivity of a metallated guest cartridge<sup>16</sup>. However, crystallographically monitoring inorganic transformations and reactions of metal complexes within a single MOF crystal remains a significant challenge. The first step towards examining inorganic chemistry within a MOF material is to determine a general strategy for the introduction of metal complexes into the pore framework with precise positional control. Post-synthetic metallation<sup>17,18</sup>, where a metal ion is inserted into a vacant coordinating site that is part of the framework structure, is an approach that has broad scope for incorporating a wide variety of metal complexes into MOFs. As this approach provides for the tethering of a metal complex in a defined position within the pore framework, it has been successfully used to enhance gas separations<sup>19–21</sup>.

and to facilitate the introduction of metal centres that catalyse reactions within the host framework<sup>22–24</sup>. Despite the wide application of post-synthetic metallation there are no examples where SCXRD has been used to unambiguously define the coordination sphere (not part of the MOF backbone) of the inserted metal. The difficulty in obtaining SCXRD information for post-synthetically metallated MOFs<sup>25,26</sup> is often attributed to diminished crystal quality, either as a result of the additional post-synthetic step or lower initial crystallinity for some chemically robust MOFs, issues with unravelling disorder in MOFs with higher crystal symmetry, and the general difficulty in achieving full site occupancy of the extraneous metal ion within the chelating moiety<sup>17,18</sup>.



Here, we describe the synthesis and characterization of a Mn(II)-based MOF, [Mn<sub>3</sub>(L)<sub>2</sub>(L')]<sup>+</sup> (1), where L and L' are crystallographically unique forms of the deprotonated ligand bis(4-(4-carboxyphenyl)-1H-3,5-dimethylpyrazolyl)methane, LH<sub>2</sub>. In the L form the carboxylate and pyrazole donors coordinate the Mn atoms of the metal node, and in the L' form only the carboxylate donors contribute to the coordination environment of the metal node, thus leaving the di-pyrazole moieties vacant within the MOF. As a consequence, L' provides a flexible di-pyrazole chelating unit poised for post-synthetic metal binding. We show that this MOF can be quantitatively metallated (confirmed by a range of techniques) with a variety of first- and second-row transition-metal ions (Co(II), Cu(II), Zn(II), Rh(I), Cd(II)) and, subsequent to this post-synthetic treatment, maintains the long-range

<sup>1</sup>School of Chemistry & Physics, Centre for Advanced Nanomaterials, The University of Adelaide, Adelaide, South Australia 5005, Australia, <sup>2</sup>Research School of Chemistry, Australian National University, Canberra, Australian Capital Territory 0200, Australia. \*e-mail: christian.doonan@adelaide.edu.au; christopher.sumby@adelaide.edu.au

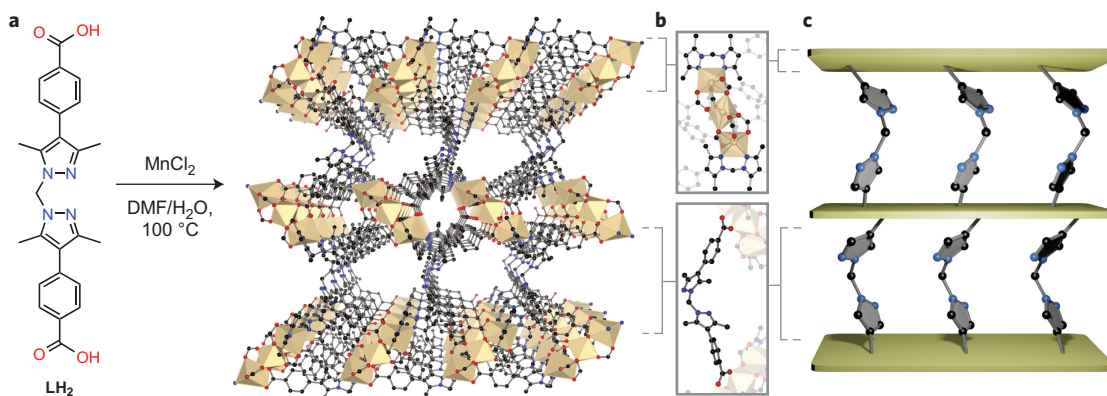


**Figure 1 | Synthesis and structural representations of MOF 1.** **a**, Synthesis of MOF 1 ( $[\text{Mn}_3(\text{L})_2(\text{L}')]$ ) from  $\text{LH}_2$  and  $\text{MnCl}_2$ , and a perspective view of the single-crystal X-ray structure of this material along the  $c$  axis. In this MOF,  $\text{L}$  and  $\text{L}'$  are structurally unique, deprotonated forms of  $\text{LH}_2$ . The  $\text{L}$  form is coordinatively saturated with both the O and N donor atoms contributing to the metal nodes of the framework. In contrast, in the  $\text{L}'$  form, only the O donor atoms coordinate to the metal node, leaving the di-pyrazole moiety vacant. Coloured spheres represent O (red), N (blue) and C (black), and the Mn centres are shown as beige polygons. **b**, Enlargements of the trinuclear Mn(II) nodes of **1** showing the coordination environment of the three Mn centres and one complete molecule of  $\text{L}'$  flanked by two trinuclear Mn(II) nodes, highlighting the pillaring ligand moiety. **c**, Schematic representation of **1** with the layers represented as mustard coloured planes and chemical detail highlighting the di-pyrazole coordinating site in  $\text{L}'$ .

order suitable for SCXRD analysis; that is, metallation occurs via a single crystal-to-single crystal (SC-SC) process. The potential of **1** to act as an isolation matrix that facilitates the observation of inorganic reaction products in the solid state was realized by using SCXRD to follow a well-known inner-sphere chemical transformation ( $O_h$  to  $T_d$  Co(II))<sup>27</sup>. Furthermore, we characterized the reaction product from the oxidative addition of  $\text{CH}_3\text{I}$  to  $\text{1}\cdot[\text{Rh}(\text{CO})_2]\text{[RhCl}_2(\text{CO})_2]$  and subsequent CO insertion into the Rh-CH<sub>3</sub> bond. The propensity of this MOF to be quantitatively metallated by a wide range of metal ions affords broad scope for studying coordinatively unusual species in the solid-state and has the potential to provide valuable structural insight into inorganic chemical reactivity and metal-based catalysis.

## Results and discussion

**Synthesis and characterization of **1**.** To facilitate the metallation process we anticipated that a MOF architecture that includes a flexible chelating group would afford greater structural degrees of freedom and thus accommodate metal ions in a wide variety of geometries in the solid-state. Accordingly, this design feature<sup>28,29</sup> was expected to give rise to higher site occupancies than a MOF constructed from rigid links. Bifunctional ligand  $\text{LH}_2$  (ref. 30) was selected as the organic building unit due to a degree of rotational freedom about the aryl-heteraryl bonds and the intrinsic flexibility provided by the central methylene bridge. Furthermore, the combination of ‘hard’ carboxylate and relatively ‘soft’ pyrazole donors could be expected, with judicious selection of reaction conditions and metal ions, to yield an open framework material replete with metal-free di-pyrazole donors.

The title material, **1**, was obtained by heating a 1.7:1  $\text{MnCl}_2/\text{LH}_2$  mixture in 6 mL of dimethylformamide (DMF)/H<sub>2</sub>O (2:1 vol. ratio) at 100 °C for 48 h. This yielded colourless, rhombic plates of  $\text{1}\cdot\text{xS}$  in 66% yield that crystallized in monoclinic space group  $P2_1/c$ . MOF **1** (Fig. 1a) is a charge-neutral three-dimensional network that can be readily envisaged as two-dimensional layers composed of trinuclear  $\text{Mn}_3(\text{II})(\text{L})_2$  nodes that are ‘pillared’ by the  $\text{L}'$  form of the ligand. Close structural analysis of **1** indicates that the Mn<sub>3</sub> node comprises a central octahedral Mn(II) atom coordinated by six carboxylate oxygen atoms and flanked by two distorted octahedral Mn(II) centres, each of which are coordinated by four oxygen donors and capped by a chelating di-pyrazole moiety (Fig. 1b).  $\text{L}'$  bridges the two-dimensional layers through the carboxylate donors, giving rise to channels measuring  $\sim 8.5 \times 10.5 \text{ \AA}$  (excluding van der Waals radii) along the  $c$  axis that are lined with vacant di-pyrazole

coordinating sites poised for post-synthetic metallation (Fig. 1b,c). The vacancy of the pyrazole moieties can be rationalized by the donor requirements for a charge-balanced  $\text{Mn}_3$  node ( $\text{Mn}_3\text{O}_{12}\text{N}_4$ ); three molecules of  $\text{L}$  provide 12 oxygen and 6 nitrogen atoms, leaving 2 non-coordinated nitrogen donors.

MOF **1** possesses exceptional structural flexibility (Fig. 2), as evidenced by gas adsorption and X-ray diffraction experiments. Powder X-ray diffraction (PXRD) patterns were collected on both the DMF exchanged (**1**-DMF) and desolvated samples (**1**-des) of **1**. Analysis of the peak positions and intensities indicated that **1** had undergone a structural transformation upon desolvation (Supplementary Fig. 14). Notably, single crystals from the desolvated sample were suitable for structure determination by SCXRD. X-ray analysis revealed that the trinuclear Mn(II) node remained essentially unchanged; however, the pillaring ligand had undergone a significant torsional rotation, resulting in a noticeably more acute bridging angle (97.5° compared to 105.1°) and thus a contraction of the two-dimensional planes (Fig. 2a). This structural contraction can be attributed to the inherent flexibility and rotational freedom of the non-coordinated  $\text{L}'$  ligand within the MOF structure. The 77 K  $\text{N}_2$  gas adsorption isotherm experiments (Fig. 3) performed on **1**-des afforded an isotherm profile with a step between  $P/P_o$  of 0.005–0.06 ( $P$  and  $P_o$  are the measured and saturation pressure of nitrogen, respectively). This is consistent with a degree of structural flexibility that probably results from rotation of the pyrazole moiety and concomitant pore enlargement<sup>31</sup>. A total  $\text{N}_2$  uptake of  $250 \text{ cm}^3 \text{ g}^{-1}$  was observed and a Brunauer–Emmett–Teller (BET) analysis of the data yielded a surface area of  $711 \text{ m}^2 \text{ g}^{-1}$ .

**Post-synthetic metallation.** Chelating pyrazole ligands are prevalent in transition-metal coordination chemistry<sup>32,33</sup>. Accordingly, the presence of a non-coordinated, structurally flexible di-pyrazole moiety within the open channels of **1** prompted us to investigate post-synthetic metallation reactions. We treated **1** with a variety of metal salts, including  $\text{CuCl}_2\cdot 2\text{H}_2\text{O}$ ,  $\text{CoCl}_2\cdot 6\text{H}_2\text{O}$ ,  $\text{Zn}(\text{NO}_3)_2\cdot 6\text{H}_2\text{O}$ ,  $[\text{Rh}(\text{CO})_2\text{Cl}]_2$  and  $\text{Cd}(\text{NO}_3)_2\cdot 6\text{H}_2\text{O}$ , and quantified the degree of metallation using inductively coupled plasma mass spectrometry (ICP-MS) and energy-dispersive X-ray analysis (EDX) (Table 1).

All metallation reactions were found to proceed in essentially quantitative yield with retention of crystallinity, as confirmed by PXRD (Supplementary Figs 15 and 16). Furthermore, for

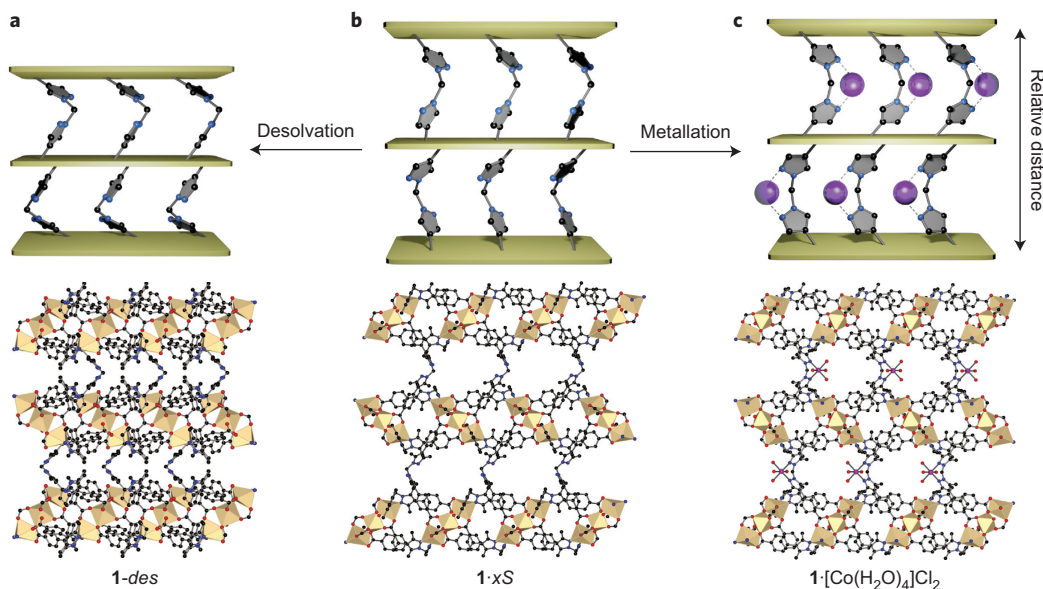


**Figure 2 | Representations of the dramatic structural flexibility displayed by 1.** **a–c,** Schematic representations and perspective views of X-ray crystal structures of different forms of **1** showing the relative layer-layer separations and highlighting the conformational changes that occur for the di-pyrazole moieties upon desolvation (**a**), for the as-synthesized MOF (**b**) and following metallation (**c**). The packing diagrams provide views of **1** showing the close-packed structure for **1-des** (along the *a* axis), the open flexible structure of **1** (along the *c* axis) and the rigid metallated form **1-[Co(H<sub>2</sub>O)<sub>4</sub>]Cl<sub>2</sub>** (along the *c* axis).

metallation with CoCl<sub>2</sub>·6H<sub>2</sub>O we studied the rate of metal ion incorporation by ICP-MS and found that the chelating sites saturated within ~3 h after a very rapid initial reaction (Supplementary Fig. 24). Quantitative metallation of MOFs is uncommon<sup>17,19,34,35</sup>, so it is noteworthy that this flexible system provides a platform for binding a wide variety of transition-metal ions with saturated binding site occupancy. A 77 K N<sub>2</sub> gas adsorption isotherm (Fig. 3) performed on **1** metallated with CoCl<sub>2</sub> yielded a Type 1 profile with a BET surface area of 1,045 m<sup>2</sup> g<sup>-1</sup>. In contrast to the non-metallated material **1-des**, the low-pressure step is not observed. These data confirm that metal coordination by the di-pyrazole moieties induces a flexible-to-rigid structural transformation (Fig. 2c). We note that such a flexible-to-rigid transformation, which is dependent on metal binding, is unprecedented in MOF chemistry.

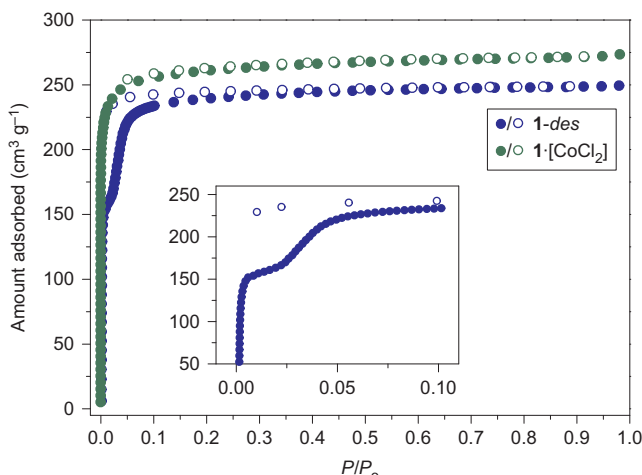


**Figure 3 | Data from the N<sub>2</sub> gas adsorption isotherm experiments performed at 77 K for **1-des** and **1-[CoCl<sub>2</sub>]**.** Inset: the step between  $P/P_0$  of 0.005–0.06 observed only for **1-des**. This step is indicative of the flexible nature of the non-metallated MOF, and the absence of this feature in the isotherm of **1-[CoCl<sub>2</sub>]** shows that metal coordination by the di-pyrazole moieties of **1** induces a flexible-to-rigid transformation in the structure.

**Observing a reversible O<sub>h</sub> to T<sub>d</sub> transformation for **1-[Co(H<sub>2</sub>O)<sub>4</sub>]Cl<sub>2</sub>** by SCXRD.** Given that **1** could be quantitatively metallated with retention of structural order in the bulk solid, we turned our efforts to obtaining SCXRD data. Deep blue crystals, formed by heating **1** in a solution of CoCl<sub>2</sub>·6H<sub>2</sub>O at 65 °C for 16 h, were utilized for SCXRD. On cooling to room temperature, the crystals became pink in colour, suggesting that a temperature-dependent transformation of the metallated species had occurred. SCXRD data collected on the pink form of the crystals were consistent with a formulation of **1-[Co(H<sub>2</sub>O)<sub>4</sub>]Cl<sub>2</sub>** (Fig. 4a), and refinement of the occupancy of the Co(II) centre supported quantitative inclusion of the Co(II) entity (Supplementary Table 3; refined Co occupancy of 93.5%). Close inspection of the structure revealed that metallation is accompanied by an *anti* to *syn* conformational switch of the pyrazole rings of the ligand (one pyrazole ring rotates ~180° to facilitate coordination), allowing chelation to the Co(II) centre. The octahedral Co(II) metal centre is situated on a mirror plane and coordinated by four water ligands (one symmetry generated, bond lengths 2.045(5)–2.158(7) Å) in addition to the two pyrazole donors of L', with a Co–N bond length of 2.159(4) Å. To our knowledge this is a novel example of

**Table 1 | Outcomes of the metallation experiments of **1** showing the product formed and extent of metallation determined by ICP-MS and EDX.**

Metal salt	Product	Percent metallation (ICP-MS)*	Percent metallation (EDX)†
CoCl <sub>2</sub> ·6H <sub>2</sub> O	<b>1-[Co(H<sub>2</sub>O)<sub>4</sub>]Cl<sub>2</sub></b>	100.0 ± 2.1	107.0 ± 4.4
CuCl <sub>2</sub> ·2H <sub>2</sub> O	<b>1-[Cu]</b>	102.0 ± 2.6	106.0 ± 4.9
Zn(NO <sub>3</sub> ) <sub>2</sub> ·6H <sub>2</sub> O	<b>1-[Zn]</b>	121.0 ± 4.0	97.7 ± 2.8
[Rh(CO) <sub>2</sub> Cl] <sub>2</sub>	<b>1-[Rh(CO)<sub>2</sub>][RhCl<sub>2</sub>(CO)<sub>2</sub>]</b>	N/A‡	99.5 ± 3.0
	<b>1-[Rh(COMe)(CO)(CH<sub>3</sub>CN)]I</b>	N/A‡	101.6 ± 8.2
Cd(NO <sub>3</sub> ) <sub>2</sub> ·6H <sub>2</sub> O	<b>1-[Cd]</b>	N/A	106.8 ± 3.6

\*ICP-MS results are the average of three samples of each material (one to two crystals per sample) and are presented with standard deviations. †EDX results are calculated as an average of at least three areas of a sample (3 mm<sup>2</sup> of crystalline sample) and presented with standard deviations.

‡Rh cannot be detected by ICP-MS. N/A, not available.

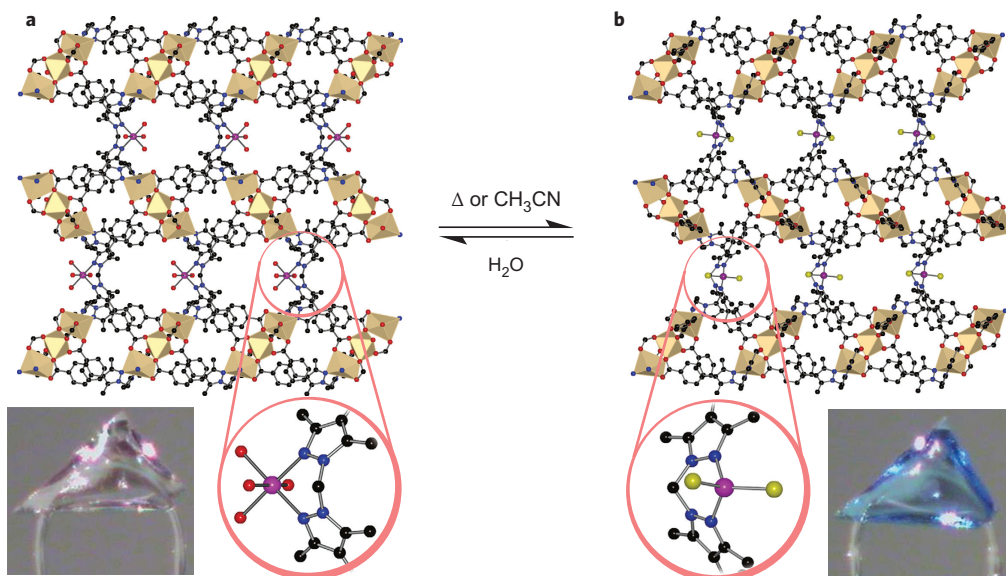


**Figure 4 | Structural details of the reversible SC-SC  $O_h$  to  $T_d$  transformation for  $\mathbf{1} \cdot [\text{Co}(\text{H}_2\text{O})_4]\text{Cl}_2$  that can be realized by heating or immersion in acetonitrile. a,** View of  $\mathbf{1} \cdot [\text{Co}(\text{H}_2\text{O})_4]\text{Cl}_2$  along the  $c$  axis showing the primary coordination sphere of the octahedral  $\text{Co}(\text{II})$  centre. Inset: a single crystal of  $\mathbf{1} \cdot [\text{Co}(\text{H}_2\text{O})_4]\text{Cl}_2$ . **b,** Structure of  $\mathbf{1} \cdot [\text{CoCl}_2]$  with a four-coordinate  $\text{Co}(\text{II})$  centre composed of the di-pyrazole site of  $\mathbf{1}$  and two chloride anions (one of two chemically identical but crystallographically independent centres shown). Inset: a single crystal of  $\mathbf{1} \cdot [\text{CoCl}_2]$ .

a post-synthetically metallated MOF where the identity, bond distances and angles of non-framework donor atoms can be determined by SCXRD.

Heating  $\mathbf{1} \cdot [\text{Co}(\text{H}_2\text{O})_4]\text{Cl}_2$  crystals to 300 K on the diffractometer engendered a distinct colour change from pink to blue. Such colour changes are well known in  $\text{Co}(\text{II})$  chemistry<sup>27</sup> and are associated with a change in the ligand field geometry from  $O_h$  to  $T_d$ . We note that a similar transformation was achieved by placing pink crystals of  $\mathbf{1} \cdot [\text{Co}(\text{H}_2\text{O})_4]\text{Cl}_2$  in dry acetonitrile. Blue crystals formed by the latter route were most suitable for SCXRD experiments (as these crystals remain solvated) and analysis of the data revealed, as anticipated, that the primary coordination sphere of the  $\text{Co}(\text{II})$  centre has a tetrahedral geometry with two coordinated chloride ligands in addition to the two nitrogen donors of  $\mathbf{L}'$  (Fig. 4b). Notably, in undergoing the SC-SC transformation from  $\mathbf{1} \cdot [\text{Co}(\text{H}_2\text{O})_4]\text{Cl}_2$  to  $\mathbf{1} \cdot [\text{CoCl}_2]$ , the  $\text{Cl}^-$  counter-ions migrate from the pores to the metal centre. Additionally, the di-pyrazole moiety of ligand  $\mathbf{L}'$  has again undergone a very significant rotation, resulting in the  $\text{Co}(\text{II})$  atom facing the opposite side of the pore when viewing the structure along the  $c$  axis. This significant movement of the post-synthetically added metal ion is testament to the flexibility of MOF  $\mathbf{1}$  and bodes well for using this material as a general platform for studying inorganic reactivity, as outlined further below. Exposure of  $\mathbf{1} \cdot [\text{CoCl}_2]$  crystals to air resulted in conversion back to the pink octahedral form after several minutes. We confirmed that this transformation was indeed consistent with the addition of four water molecules to the cobalt coordination sphere by elemental analysis.

**Observing the outcome of chemical reactions by SCXRD.** We sought to extend the potential of the platform material MOF  $\mathbf{1}$  to observing chemical products of Rh-centred reactions in the solid state. Given that Rh complexes are extensively used in homogeneous catalysis, structural insight into their chemistry is of significant fundamental and practical interest. Accordingly, as a proof of principle that reaction products can be structurally elucidated in the MOF pores,  $\mathbf{1}$  (Fig. 5a) was treated with

$[\text{Rh}(\text{CO})_2\text{Cl}]_2$  in dry acetonitrile at room temperature for 48 h. SCXRD studies readily confirmed that the Rh(i) species formed was  $\mathbf{1} \cdot [\text{Rh}(\text{CO})_2][\text{RhCl}_2(\text{CO})_2]$ , where the Rh(i) centre (91% refined occupancy) assumes the expected square planar geometry (Fig. 5b) consisting of two nitrogen donors from the di-pyrazole unit and two carbonyl ligands (Rh-C bond length 1.844(11) Å, consistent with previously reported Rh-C bond lengths for similar compounds)<sup>36</sup>. In addition, a square planar  $[\text{RhCl}_2(\text{CO})_2]^-$  counter-ion was located within the pores of the MOF<sup>37</sup>. Characteristic Fourier transform infrared stretches<sup>36,37</sup> were observed for  $\mathbf{1} \cdot [\text{Rh}(\text{CO})_2][\text{RhCl}_2(\text{CO})_2]$  with five CO bands observed at 2,106, 2,075, 2,046, 2,033 and 2,002 cm<sup>-1</sup> (Supplementary Fig. 1). It is noteworthy that when aqueous methanol was used in air to effect metallation, a different and unusual Rh(III) species  $\mathbf{1} \cdot [\text{Rh}(\text{H}_2\text{O})_4]\text{Cl}_3$  was characterized by SCXRD (Fig. 5d). Formation of a related octahedral Rh(III) species could also be achieved via a SC-SC transformation by exposing  $\mathbf{1} \cdot [\text{Rh}(\text{CO})_2][\text{RhCl}_2(\text{CO})_2]$  to water (1:1 MeOH/water) and air over extended periods. It is worth noting that full conversion to the oxidized Rh(III) species takes three months at room temperature to occur within the framework, suggesting that the MOF architecture stabilizes these metal sites towards hydrolysis.

Further treatment of  $\mathbf{1} \cdot [\text{Rh}(\text{CO})_2][\text{RhCl}_2(\text{CO})_2]$  in  $\text{CH}_3\text{CN}$  with MeI vapour resulted in a noticeable colour change of the crystals from bright yellow to bright orange (Supplementary Fig. 13). The orange colour is consistent with a Rh(III) species and hence suggested that oxidative addition of the halo-alkane to the Rh(i) complex had occurred. The SC-SC transformation was confirmed by SCXRD, which showed that the Rh(i) complex (95% refined occupancy) had undergone both an oxidative addition of MeI to give the methyl iodide adduct and a subsequent insertion (methyl migration) reaction of one of the CO ligands into the newly formed Rh-Me bond. This migration leaves a vacant coordination site on the octahedral Rh(III), which allows coordination by a solvent (acetonitrile) molecule (Fig. 5c). In  $\mathbf{1} \cdot [\text{Rh}(\text{CO})(\text{CH}_3\text{CN})(\text{COMe})\text{I}]$ , the Rh(III) metal centre adopts an octahedral geometry with the CO and  $\text{CH}_3\text{CN}$  ligands in the same plane as the nitrogen

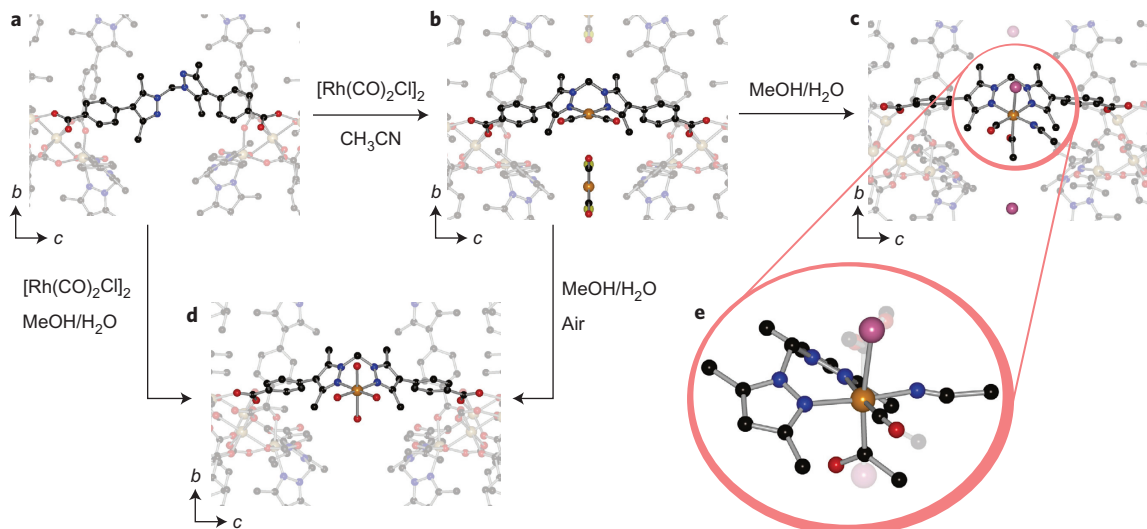


**Figure 5 | Reaction scheme showing X-ray crystallographic snapshots along the *a* axis of 1 treated with  $[\text{Rh}(\text{CO})_2\text{Cl}]_2$  and subsequent oxidative reactions.** **a–e**, Structure of 1 before treatment with  $[\text{Rh}(\text{CO})_2\text{Cl}]_2$  (**a**), 1-[ $\text{Rh}(\text{CO})_2$ ] $[\text{RhCl}_2(\text{CO})_2]$  (**b**), 1-[ $\text{Rh}(\text{CO})(\text{CH}_3\text{CN})(\text{COMe})\text{I}$ ]I (**c**) and 1-[ $\text{Rh}(\text{H}_2\text{O})_4\text{Cl}_3$ ] (**d**) (selected bond lengths in Å: Rh–O 2.080(5), 2.084(11) and 2.271(8)), and a view of the Rh(III) centre of 1-[ $\text{Rh}(\text{CO})(\text{CH}_3\text{CN})(\text{COMe})\text{I}$ ]I (**e**) showing the other positions of the disorder model as faded atoms.

donors of the pyrazole rings, while the iodide and the  $\text{C}(=\text{O})\text{Me}$  moieties occupy the axial positions (Fig. 5e).

Evidence for iodide (as opposed to chloride) ligands bound to the Rh(III) centre comes from the relative size of the peaks in the difference electron density maps, the Rh–X bond lengths (2.982(2) and 3.008(5) Å), which lie well within the range expected for Rh–I bonds (Supplementary Fig. 12), and EDX analysis, which confirms the expected Mn:Rh:I ratio of 3:1:2 (Supplementary Table 6). The square planar  $[\text{Rh}(\text{CO})_2\text{Cl}_2]^-$  counter-ion of the starting material is displaced during the course of this SC–SC reaction, as it is also known to react with MeI<sup>38,39</sup>. The presence of the CO and COMe ligands, as well as the absence of the  $[\text{Rh}(\text{CO})_2\text{Cl}_2]^-$  counter-ion, were further supported by infrared spectroscopy (Supplementary Fig. 1), with only one CO band remaining at  $2,072\text{ cm}^{-1}$  and a new band appearing at  $1,716\text{ cm}^{-1}$  corresponding to the  $\text{C}(=\text{O})\text{Me}$  group<sup>40,41</sup> (these are broadened as they relate to the four isomers of the Rh(III) complex present in the MOF). This type of chemistry has been observed for rhodium, but no direct observation of such products containing this donor set has hitherto been accomplished by SCXRD<sup>40</sup>. In this case, significantly, including the initial metallation of the MOF, a total of three sequential chemical reactions were carried out in quantitative yield within the MOF without loss of single crystallinity or leaching of Rh (Table 1). We also note that these are the first examples of the products of oxidation reactions being elucidated within a MOF crystal by SCXRD.

To provide mechanistic insight into the reaction that gave the crystallographically observed product 1-[ $\text{Rh}(\text{CO})(\text{CH}_3\text{CN})(\text{COMe})\text{I}$ ]I, a density functional theory study of the reaction of a simplified model of the Rh(I) starting material with  $\text{CH}_3\text{I}$  in acetonitrile solution was conducted (see Supplementary Section 12). Calculations were performed at the M11-L/6-31G(d,p) + SDD level of theory in conjunction with the SMD solvent model, where M11 is a dual-range functional that has been shown to provide excellent accuracy for organometallic chemistry and MOFs<sup>42,43</sup>. The calculated mechanism indicates the reaction proceeds via an  $\text{S}_{\text{N}}2$  attack on MeI by the Rh(I) species<sup>44</sup>. This oxidative addition step is found to be facilitated by the presence of the  $[\text{Rh}(\text{Cl})_2(\text{CO})_2]^-$  counter-ion, which renders the Rh(I) species more nucleophilic. The reaction is completed by a methyl migration to yield the crystallographically observed reaction product 1-[ $\text{Rh}(\text{CO})(\text{CH}_3\text{CN})(\text{COMe})\text{I}$ ]I. The geometries can be compared with the corresponding experimental values; in both cases, for the

starting 1-[ $\text{Rh}(\text{CO})_2$ ] $[\text{RhCl}_2(\text{CO})_2]$  species and the final product 1-[ $\text{Rh}(\text{CO})(\text{CH}_3\text{CN})(\text{COMe})\text{I}$ ]I, the key structural parameters lie within  $\pm 0.1\text{ \AA}$  of experimentally refined values (see Supplementary Information). Furthermore, the stretching frequencies calculated for the final product ( $2,227\text{ cm}^{-1}$ ,  $1,900\text{ cm}^{-1}$ ) show qualitative agreement with the experimental values ( $2,072\text{ cm}^{-1}$  [CO],  $1,716\text{ cm}^{-1}$  [COMe]), although with a shift of  $\sim 150\text{--}180\text{ cm}^{-1}$  due to the anchoring effect of the MOF, which is neglected (by necessity) in the calculations.

## Conclusions

A key structural feature of 1 is the flexibility of the chelating pyrazole donors, which predispose the material to binding a broad range of transition-metal ions and, importantly, accommodate the geometric rearrangements associated with metal-centred chemical reactions undertaken on the framework. The full extent of this structural flexibility is captured by the dramatic structural rearrangement of the L' backbone that occurs when 1-[ $\text{Co}(\text{H}_2\text{O})_4\text{Cl}_2$ ] is transformed into 1-[ $\text{CoCl}_2$ ]; during this reaction the di-pyrazole moiety flips nearly  $180^\circ$  within the MOF and this occurs with retention of crystallinity. The ultimate outcome of this structural feature for the following chemistry within MOF 1 is that potential strain on the framework backbone is minimized. We posit this leads to preservation of the high degree of crystallinity described in each instance. In addition, close inspection of the metallated forms of 1 reveals that each pore hosts only a single framework-bound coordination site. This structural element alleviates the likely steric congestion that would undoubtedly diminish the capacity to explore reaction chemistry within the pore network in materials of higher symmetry<sup>45,46</sup>. Furthermore, the lower crystal symmetry (primitive monoclinic) minimizes the crystallographic challenges associated with following reactions within the MOF pores.

In summary, we have synthesized a new MOF that is poised for post-synthetic metallation via the free chelating di-pyrazole moieties lining its pores. Remarkably, in the case of metallating the MOF with Rh(I) and subsequent addition of MeI, we were able to observe the reaction products of three consecutive chemical transformations within the pores of 1 by SCXRD. These data clearly show that MOF 1 is a unique platform that can be utilized to determine the structures of unusual species in the solid-state or elucidate valuable structural information pertaining to metal-based catalysis.

## Methods

**SCXRD studies.** Single crystals were mounted in paratone-N oil on a nylon loop. X-ray diffraction data were collected at 150(2) K with Mo K $\alpha$  radiation ( $\lambda = 0.7107 \text{ \AA}$ ) using an Oxford Diffraction X-calibur single-crystal X-ray diffractometer (1-des and 1-[Co(H<sub>2</sub>O)<sub>4</sub>]Cl<sub>2</sub>) or at 100(2) K on the MX-1 beamline of the Australian Synchrotron ( $\lambda = 0.7107 \text{ \AA}$ ). Data sets were corrected for absorption using a multi-scan method, and structures were solved by direct methods using SHELXS-97<sup>46</sup> and refined by full-matrix least squares on  $F^2$  by SHELXL-97 (ref. 47), interfaced through the program X-Seed<sup>48</sup>. In general, all non-hydrogen atoms were refined anisotropically and hydrogen atoms were included as invariants at geometrically estimated positions, unless specified otherwise in Supplementary section 'Additional details'. Full details of the structure determinations have been deposited with the Cambridge Crystallographic Data Centre as CCDC nos. 989581–989587 (specifically CCDC 989581, 1-DMF; CCDC 989582, 1-des; CCDC 989583, 1-[Co(H<sub>2</sub>O)<sub>4</sub>]Cl<sub>2</sub>; CCDC 989584, 1-[CoCl<sub>2</sub>]; CCDC 989585, 1-[Rh(CO)<sub>2</sub>][RhCl<sub>2</sub>(CO)<sub>2</sub>]; CCDC 989586, 1-[Rh(H<sub>2</sub>O)<sub>4</sub>]Cl<sub>3</sub>; CCDC 989587, 1-[Rh(CO)(CH<sub>3</sub>CN)(COMe)]I). Copies of this information may be obtained free of charge.

**1-[Co(H<sub>2</sub>O)<sub>4</sub>]Cl<sub>2</sub>.** All atoms from the framework and the post-synthetically added metal complex were refined with anisotropic displacement parameters (Supplementary Fig. 6 shows a thermal ellipsoid plot with the ellipsoids shown at the 50% probability level), with the ligands and donor atoms coordinated to the Co centre identified by peak heights and comparison to bond length data obtained from the Cambridge Structural Database (Supplementary Fig. 11, CSD Version 5.35, release date November 2013). The Co–O bond lengths observed (2.045(5), 2.126(4) and 2.158(7)  $\text{\AA}$ ) are well within the range typically seen for octahedral Co(II) complexes.

**1-[CoCl<sub>2</sub>].** Again, all atoms from the framework and the post-synthetically added metal species could be refined with anisotropic displacement parameters (Supplementary Fig. 7 shows a thermal ellipsoid plot with the ellipsoids shown at the 50% probability level). The identity of the coordinated atoms was determined from the relative peak heights in the electron density maps and by consideration of the bond lengths for the Co–X (X = O or Cl) bonds as compared to data extracted from the CSD (Supplementary Fig. 11, CSD Version 5.35, release date November 2013). In this manner the two coordinated atoms were identified as Cl and further evidence for their presence was obtained by elemental and EDX analysis.

**1-[Rh(CO)<sub>2</sub>][RhCl<sub>2</sub>(CO)<sub>2</sub>].** Once again, all framework atoms and those of the post-synthetically incorporated metal could be refined with anisotropic displacement parameters (Supplementary Fig. 8 shows a thermal ellipsoid plot with the ellipsoids shown at the 50% probability level).

**1-[Rh(H<sub>2</sub>O)<sub>4</sub>]Cl<sub>3</sub>.** SCXRD confirmed the rhodium species (88% refined occupancy) to be octahedral with four isolated elliptical regions of electron density located  $\sim 2 \text{ \AA}$  from the Rh centre (Supplementary Fig. 25). These peaks in the difference map were assigned as water ligands and, despite not being able to locate the hydrogen atoms, were satisfactorily refined as water molecules (Supplementary Fig. 9 shows a thermal ellipsoid plot with the ellipsoids shown at the 50% probability level). The anions could not be located but their presence in the lattice was supported by elemental analysis as chloride.

**1-[Rh(CO)(CH<sub>3</sub>CN)(COMe)]I.** As the Rh(I) species in 1-[Rh(CO)<sub>2</sub>][RhCl<sub>2</sub>(CO)<sub>2</sub>] can undergo initial reaction from either above or below, two arrangements for the iodide and methyl ligands are possible, and these two intermediates can further undergo methyl migration onto one of the two CO groups. This generates four possible isomers of the final product, which are disordered across a mirror plane. The two positions of the disordered iodide ligands are readily evident from the difference electron density maps, with two large peaks appearing in the range 2.9–3.0  $\text{\AA}$  above and below the N–Rh–N plane. Similarly, disorder of the CO/CH<sub>3</sub>CN ligands in the N–Rh–N plane could also be identified in this manner with two peaks (CO/NC) of higher electron density in close proximity and a third, lower peak (CH<sub>3</sub>)  $\sim 1.5 \text{ \AA}$  from the second. Using  $F_{\text{obs}}$  (observed structure-factor amplitude) electron density plots, which provide evidence for a three-atom species, that is, the acetyl group (Supplementary Fig. 26), a disorder model could be developed and refined against the data (Supplementary Fig. 10 shows a thermal ellipsoid plot with the ellipsoids shown at the 50% probability level). Due to the proximity of the iodide and acetyl ligands and the significant electron density associated with the iodide anions, the disordered acetyl moieties were placed in calculated positions and refined with coordinates, site occupancy factors (s.o.f.) and isotropic displacement parameters (U) fixed (the latter at 0.15).

Received 23 March 2014; accepted 24 July 2014;  
published online 7 September 2014

## References

- Ooi, L. *Principles of X-ray Crystallography* (Oxford Univ. Press, 2010).
- Sheldrick, G. M. A short history of SHELX. *Acta Crystallogr. A* **64**, 112–122 (2008).
- Inokuma, Y. *et al.* X-ray analysis on the nanogram to microgram scale using porous complexes. *Nature* **495**, 461–466 (2013); *ibid.* Corrigendum. *Nature* **501**, 262 (2013).
- Legrand, Y.-M., van der Lee, A. & Barboiu, M. Single-crystal X-ray structure of 1,3-dimethylcyclobutadiene by confinement in a crystalline matrix. *Science* **329**, 299–302 (2010).
- Inokuma, Y., Kawano, M. & Fujita, M. Crystalline molecular flasks. *Nature Chem.* **3**, 349–358 (2011).
- Kawamichi, T., Haneda, T., Kawano, M. & Fujita, M. X-ray observation of a transient hemiaminal trapped in a porous network. *Nature* **461**, 633–635 (2009).
- Haneda, T., Kawano, M., Kawamichi, T. & Fujita, M. Direct observation of the labile imine formation through single-crystal-to-single-crystal reactions in the pores of a porous coordination network. *J. Am. Chem. Soc.* **130**, 1578–1579 (2008).
- Haneda, T., Kawano, M., Kojima, T. & Fujita, M. Thermo-to-photo switching of the chromic behavior of salicylideneanilines via inclusion in a porous coordination network. *Angew. Chem. Int. Ed.* **46**, 6643–6645 (2007).
- Kawano, M., Kobayashi, Y., Ozeki, T. & Fujita M. Direct crystallographic observation of a coordinatively unsaturated transition-metal complex *in situ* generated within a self-assembled cage. *J. Am. Chem. Soc.* **128**, 6558–6559 (2006).
- Kohyama, Y., Murase, T. & Fujita, M. Metal–organic proximity in a synthetic pocket. *J. Am. Chem. Soc.* **136**, 2966–2969 (2014).
- Zhang, J.-P. & Chen, X.-M. Optimised acetylene/carbon dioxide sorption in a dynamic porous crystal. *J. Am. Chem. Soc.* **131**, 5516–5521 (2009).
- Takamizawa, S. *et al.* Crystal transformation and host molecular motions in CO<sub>2</sub> adsorption process of a metal benzoate pyrazine (M=Rh, Cu). *J. Am. Chem. Soc.* **132**, 3783–3792 (2010).
- Vaidhyanathan, R. *et al.* Direct observation and quantification of CO<sub>2</sub> binding within an amine-functionalized nanoporous solid. *Science* **330**, 650–653 (2010).
- Rowell, J. L. C., Spenser, E. C., Eckert, J., Howard, J. A. K. & Yaghi, O. M. Gas adsorption sites in a large-pore metal–organic framework. *Science* **309**, 1350–1354 (2005).
- Vinogradova, E. V., Müller, P. & Buchwald, S. L. Structural reevaluation of the electrophilic hypervalent iodine reagent for trifluoromethylthiolation supported by the crystalline sponge method for X-ray analysis. *Angew. Chem. Int. Ed.* **126**, 3189–3192 (2014).
- Ikemoto, K., Inokuma, Y., Rissanen, K. & Fujita, M. X-ray snapshot observation of palladium-mediated aromatic bromination in a porous complex. *J. Am. Chem. Soc.* **136**, 6892–6895 (2014).
- Cohen, S. M. Postsynthetic methods for the functionalization of metal–organic frameworks. *Chem. Rev.* **112**, 970–1000 (2012).
- Evans, J. D., Sumby, C. J. & Doonan, C. J. Post-synthetic metalation of metal–organic frameworks. *Chem. Soc. Rev.* **43**, 5933–5951 (2014).
- Bloch, E. D. *et al.* Metal insertion in a microporous metal organic framework lined with 2,2'-bipyridine. *J. Am. Chem. Soc.* **132**, 14382–14384 (2010).
- Bohsack, A. M., Ibarra, I. A., Bakhmutov, V. I., Lynch, V. M. & Humphrey, S. M. Rational design of porous coordination polymers based on bis(phosphine)MCl<sub>2</sub> complexes that exhibit high-temperature H<sub>2</sub> sorption and chemical reactivity. *J. Am. Chem. Soc.* **135**, 16038–16041 (2013).
- Mulfort, K. L., Farha, O. K., Stern, C. L., Sarjeant, A. A. & Hupp, J. T. Post-synthesis alkoxide formation within metal–organic framework materials: a strategy for incorporating highly coordinatively unsaturated metal ions. *J. Am. Chem. Soc.* **131**, 3866–3868 (2009).
- Ma, L., Falkowski, J. M., Abney, C. & Lin, W. A series of isoreticular chiral metal–organic frameworks as a tunable platform for asymmetric catalysis. *Nature Chem.* **2**, 838–846 (2010).
- Canivet, J., Aguado, S., Schuurman, Y. & Farrusseng, D. MOF-supported selective ethylene dimerization single-site catalysts through one-pot postsynthetic modification. *J. Am. Chem. Soc.* **135**, 4195–4198 (2013).
- Wu, C.-D., Hu, A., Zhang, L. & Lin, W. A homochiral porous metal organic framework for highly enantioselective heterogeneous asymmetric catalysis. *J. Am. Chem. Soc.* **127**, 8940–8941 (2005).
- Dau, P. V., Kim, M. & Cohen, S. M. Site-selective cyclometalation of a metal–organic framework. *Chem. Sci.* **4**, 601–605 (2013).
- Jacobs, T., Clowes, R., Cooper, A. I. & Hardie, M. J. A chiral, self-catenating and porous metal–organic framework and its post-synthetic metal uptake. *Angew. Chem. Int. Ed.* **51**, 5192–5195 (2012).
- Cotton, F. A. & Wilkinson, G. *Advanced Inorganic Chemistry* (Wiley, 1988).
- Bloch, W. M. & Sumby, C. J. Guest-induced crystal-to-crystal expansion and contraction of a 3-D porous coordination polymer. *Chem. Commun.* **48**, 2534–2536 (2012).
- Bloch, W. M., Babarao, R., Hill, M. R., Doonan, C. J. & Sumby, C. J. Post-synthetic structural processing in a metal–organic framework material as a mechanism for exceptional CO<sub>2</sub>/N<sub>2</sub> selectivity. *J. Am. Chem. Soc.* **135**, 10441–10448 (2013).
- Bloch, W. M., Doonan, C. J. & Sumby, C. J. Using hinged ligands to target structurally flexible copper(II) MOFs. *CrystEngComm* **15**, 9663–9671 (2013).

31. Keene, T. D. *et al.* Solvent-modified dynamic porosity in chiral 3D kagome frameworks. *Dalton Trans.* **42**, 7871–7879 (2013).
32. Pettinari, C., Santini, C., Leonesi, D., Cecchi, P. Synthesis and characterization of some zinc, cadmium and mercury(II) derivatives of bis(4-methylpyrazol-1-yl) alkane. *Polyhedron* **13**, 1553–1562 (1994).
33. Trofimenko, S. Coordination chemistry of pyrazole-derived ligands. *Chem. Rev.* **72**, 497–509 (1972).
34. Shultz, A. M., Sarjeant, A. A., Farha, O. K., Hupp, J. T. & Nguyen, S. T. Post-synthesis modification of a metal-organic framework to form metallosalen-containing MOF materials. *J. Am. Chem. Soc.* **133**, 13252–13255 (2011).
35. Morris, W. *et al.* Synthesis, structure, and metalation of two new highly porous zirconium metal-organic frameworks. *Inorg. Chem.* **51**, 6443–6445 (2012).
36. Teuma, E. *et al.* Tandem carbonylation reactions: hydroformylation and hydroaminomethylation of alkenes catalyzed by cationic  $[(\text{H}_2\text{C}(3,5-\text{Me}_2\text{Pz})_2)\text{Rh}(\text{CO})\text{L}]^+$  complexes. *Organometallics* **22**, 5261–5267 (2003).
37. Oro, L. A. *et al.* Rhodium(I) complexes with bis(pyrazolyl)methane crystal structure of  $[\text{Rh}(\text{COD})(\text{CH}_2\text{Pz})_2]\text{ClO}_4 \cdot \frac{1}{2} \text{C}_2\text{H}_4\text{Cl}_2$ . *J. Organomet. Chem.* **276**, 79–97 (1984).
38. Ellis, P. R. *et al.* Oxidative addition of alkyl halides to rhodium(I) and iridium(I) dicarbonyl diiodides: key reactions in the catalytic carbonylation of alcohols. *Organometallics* **13**, 3215–3226 (1994).
39. Nguyen, D. H. *et al.* Reductive elimination of anhydrides from anionic iodo acetyl carboxylato rhodium complexes. *Eur. J. Inorg. Chem.* **2014**, 326–336 (2014).
40. Conifer, C. M. *et al.* Dicarbonylrhodium(I) complexes of bipyridine ligands with proximate H-bonding substituents and their application in methyl acetate carbonylation. *Eur. J. Inorg. Chem.* **2011**, 3511–3522 (2011).
41. Montag, M. *et al.* CO-induced methyl migration in a rhodium thiophosphoryl pincer complex and its comparison with phosphine-based complexes: the divergent effects of S and P donor ligands. *Organometallics* **32**, 7163–7180 (2013).
42. Peverati, R. & Truhlar, D. G. M11-L: a local density functional that provides improved accuracy for electronic structure calculations in chemistry and physics. *J. Phys. Chem. Lett.* **3**, 117–124 (2012).
43. Lee, K. *et al.* Design of a metal-organic framework with enhanced back bonding for separation of  $\text{N}_2$  and  $\text{CH}_4$ . *J. Am. Chem. Soc.* **136**, 698–704 (2013).
44. Feliz, M., Freixa, Z., van Leeuwen, P. W. N. M. & Bo, C. Revisiting the methyl iodide oxidative addition to rhodium complexes: a DFT study of the activation parameters. *Organometallics* **24**, 5718–5723 (2005).
45. Ingleson, M. J., Barrio, J. P., Guilbaud, J.-P., Khimyak, Y. Z. & Rosseinsky, M. J. Framework functionalisation triggers metal binding. *Chem. Commun.* 2680–2682 (2008).
46. Sheldrick, G. M. Phase annealing in SHELX-90: direct methods for larger structures. *Acta Crystallogr. A* **46**, 467–473 (1990).
47. Sheldrick, G. M. *SHELXL-97* (University of Göttingen, 1997).
48. Barbour, L. J. A software tool for supramolecular crystallography. *J. Supramol. Chem.* **1**, 189–191 (2001).

## Acknowledgements

C.J.D. and C.J.S. acknowledge the Science and Industry Endowment Fund for financial support and the Australian Research Council for funding Future Fellowships (FT100100400 and FT0991910). Aspects of this research were undertaken on the MX1 and MX2 beamlines at the Australian Synchrotron, Victoria, Australia. M.L.C. acknowledges generous allocations of supercomputing time on the National Facility of the National Computational Infrastructure and an ARC Future Fellowship (FT100100320). Correspondence and requests for materials should be addressed to C.J.D. and C.J.S.

## Author contributions

All authors contributed extensively to the work presented in this paper. W.M.B. and A.B. undertook most of the synthetic work and analysis. C.J.C. measured and interpreted the ICP-MS data. W.M.B., A.B., C.J.C. and C.J.S. collected, solved and refined the SCXRD data. R.L. and M.L.C. undertook the computational studies. W.M.B., C.J.D. and C.J.S. wrote the manuscript with input from the other authors.

## Additional information

Supplementary information is available in the online version of the paper. Reprints and permissions information is available online at [www.nature.com/reprints](http://www.nature.com/reprints). Correspondence and requests for materials should be addressed to C.J.D. and C.J.S.

## Competing financial interests

The authors declare no competing financial interests.